

T-Matrix light scattering simulation of rough, non-symmetrical spherical particles

Jens Hellmers^{a,*}, Thomas Wriedt^b

^aUniversität Bremen, Badgasteiner Str. 3, 28359 Bremen, Germany

^bInstitut für Werkstofftechnik, Badgasteiner Str. 3, 28359 Bremen, Germany

Abstract

Light scattering is an useful tool for the detection and characterization of different types of particles and simulation of the scattering process can help to understand the scattering characteristics. To simplify the computational simulation often axis-symmetric particles are used, while in reality particles usually do not show such simple structures. To cope with this, advanced methods and algorithms are needed. In this paper we investigate the scattering characteristics by spherical particles with a rough surface, which therefore are non-symmetrical. The light scattering diagrams by these complex structured particles are computed using the nullfield method with discrete sources. The particle shape data is generated by computational methods; here we use the concept of Gardner Series to create spherical particles with a rough surface.

© 2007 Elsevier Ltd. All rights reserved.

Keywords: Nullfield method with discrete sources; T-Matrix; Rough particles

1. Introduction

Light scattering is applied to the detection and characterization of several types of particles: artificial aerosol particles such as asbestos or glass fibers [1], biological cells, natural aerosol particles [2], interstellar dust [3] or technical microparticles. Light scattering simulation can help to understand the corresponding characteristics, and for this sophisticated simulation algorithms are needed. As the simulation of real-shaped particles is either complex or time consuming, investigations are often limited to rotational symmetrical particles like spheres, spheroids and finite cylinders. Over the years now less trivial shapes have been examined, for example by Doicu for ellipsoids [4], Laitinen for cubes [5] and Wriedt for superellipsoids [6]. Additionally we would like to mention measured data by Volten [7]. Reconstruction of shapes for scattering computation was done by Kocifai [8] for an interstellar dust particle, while Wriedt reconstructed the shape of a pebble [6]. In this paper we would like to do another investigation for light scattering studies by realistically shaped particles. For this we use a new approach to create rough particle shape data and investigate the corresponding light scattering. Rough particles can be found in a variety of research fields. For example as biological particles such as erythrocyte [10], spores [11], leukocyte [12] or pollen [13].

*Corresponding author. Tel.: +49 421 2185418; fax: +49 421 2185378.

E-mail address: hellmers@iwt.uni-bremen.de (J. Hellmers).

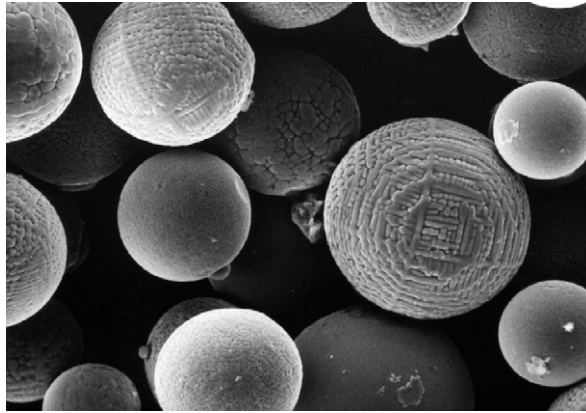


Fig. 1. Rough particles generated by metal spraying.

This paper presents results for investigations regarding to light scattering by single metal particles generated by spraying. The spray of this process consists of metallic spheres with a more or less rough surface, see Fig. 1.

For the light scattering simulation for such kind of particles we intend to use three-dimensional models consisting of triangular surface patches, reconstructed from the particle's shape. To get a first impression of the influence of the rough surface on light scattering in general, we use shape models created by computer.

Over the years several approaches were used to study light scattering by stochastically shaped particles theoretically. An extensive overview about this was given by Muinonen [14]. A popular approach to create a rough surface on a particle is the Gaussian random particle, see Muinonen [15]. Similar work has been done for example by Li et al. [16].

For our work we prefer an approach where a three-dimensional grid model describing the particle shape is used. So for preliminary investigations a routine is needed to create such files, corresponding to that models we would get from reconstruction of a real shape. For this we use the *HyperFun* Polygonizer [17]. This program offers a routine by that the surface of a given geometrical object can be interfered with solid noise. The result is a 'mutated' particle which former smooth surface becomes rough. The advantage of the *HyperFun* Polygonizer is that it enables to create an output file containing the three-dimensional structure of the particle, which is comparable to reconstructed, three-dimensional particle data. Using particles generated by the *HyperFun* Polygonizer light scattering simulations are done; in this way our work is a preliminary study for investigations using reconstructed real shapes. These scattering computations will be based on the nullfield method with discrete sources (NFM-DS). The theory will be explained in the first part of the paper. It is followed by a description how the rough particle input data was generated. Finally exemplary results for different questions regarding to the rough particles are presented.

2. Nullfield method with discrete sources

The classical T-matrix method was introduced by Waterman [18] and is also known as nullfield method (NFM) or extended boundary condition method (EBCM). It is based on an expansion of the incident, transmitted and the scattered field into a series of spherical vector wave functions (SVWF). Over the years it became a popular method, especially as fast computer codes are easily available, e.g. by Barber [19] or Mishchenko [20]. Usually most of these programs are restricted to scattering by simple particle shapes; for extreme geometries or particles with appreciable concavities the single spherical coordinate-based NFM fails to converge. To cope with this limitations and to improve numerical stability a number of modifications to the conventional NFM have been applied. One of these modifications is the NFM-DS, which was developed by Doicu et al. [21,22]. Here a number of elementary, discrete sources approximate the surface current densities. They are placed in an additional region with respect to the region where the solution is required. The amplitudes which produce the surface densities are computed by using the nullfield condition of the total electric field inside the particle surface. The NFM-DS allows to compute light scattering by elongated fibers

[23] and flat discs [24] of high aspect ratios, concave Cassini-shaped particles [25] and layered particles [26]. Additionally the NFM-DS has been extended for scattering computation by non-axisymmetric scatterers [27] and the method has been validated by comparison to other methods [28] giving results for cubes. The main characteristic and biggest advantage of the method is that the T-matrix can be computed for post-processing such as cluster scattering or orientation averaging.

The mathematical formulation of the scattering problem of an incident field $(\mathbf{E}_0, \mathbf{H}_0)$ by a homogeneous dielectric object with surface S consists of Maxwell's equations

$$\nabla \times \mathbf{E}_t = jk\mu_t \mathbf{H}_t, \quad \nabla \times \mathbf{H}_t = -jk\varepsilon_t \mathbf{E}_t \quad (1)$$

in Ω_t , $t = s, i$, the boundary conditions on the particle surface

$$\mathbf{n} \times (\mathbf{E}_0 + \mathbf{E}_s - \mathbf{E}_i) = 0, \quad \mathbf{n} \times (\mathbf{H}_0 + \mathbf{H}_s - \mathbf{H}_i) = 0 \quad (2)$$

on S , \mathbf{n} is the outward unit normal to S , $\varepsilon_s, \mu_s > 0$, and the radiation condition for $(\mathbf{E}_s, \mathbf{H}_s)$ uniformly over all possible radial directions. The scattered field $\mathbf{E}_s, \mathbf{H}_s$ must satisfy the Silver–Müller radiation condition uniformly for all directions \mathbf{x}/x so that the transmission boundary-value problem possesses an unique solution [29]. The scattering object is replaced by a set of surface current densities \mathbf{e} and \mathbf{h} , so that in the exterior domain the sources and fields match those existing in the original scattering problem. A set of integral equations for the surface current densities \mathbf{e} and \mathbf{h} is derived for a variety of discrete sources so that the nullfield condition within D_i is guaranteed. Depending on the specific scattering problem localized vector spherical functions, distributed vector spherical functions, magnetic and electric dipoles or vector Mie-potentials can be used [21]. The NFM-DS consists in the projection relations

$$\begin{aligned} \int_S \left[(\mathbf{e} - \mathbf{e}_0) \cdot \Psi_v^3 + j\sqrt{\frac{\mu_s}{\varepsilon_s}} (\mathbf{h} - \mathbf{h}_0) \cdot \Phi_v^3 \right] dS &= 0, \\ \int_S \left[(\mathbf{e} - \mathbf{e}_0) \cdot \Phi_v^3 + j\sqrt{\frac{\mu_s}{\varepsilon_s}} (\mathbf{h} - \mathbf{h}_0) \cdot \Psi_v^3 \right] dS &= 0, \quad v = 1, 2, \dots \end{aligned} \quad (3)$$

with $\mathbf{e}_0 = \mathbf{n} \times \mathbf{E}_0$ and $\mathbf{h}_0 = \mathbf{n} \times \mathbf{H}_0$ as tangential components of the incident fields. The set $\{\Psi_v^3, \Phi_v^3\}_{v=1,2,\dots}$ consists of radiating solutions to Maxwell equations and thereby depends on the system of discrete sources used for imposing the nullfield condition. Here localized vector spherical functions $\{\mathbf{M}_{mn}^{1,3}, \mathbf{N}_{mn}^{1,3}\}_{m \in \mathbb{Z}, n \geq \max(1, |m|)}$ are used

$$\begin{aligned} \mathbf{M}_{mn}^{1,3}(k\mathbf{x}) &= \sqrt{D_{mn} z_n(kr)} \left[jm \frac{P_n^{|m|}(\cos \theta)}{\sin \theta} \mathbf{e}_\theta - \frac{dP_n^{|m|}(\cos \theta)}{d\theta} \mathbf{e}_\varphi \right] e^{jm\varphi}, \\ \mathbf{N}_{mn}^{1,3}(k\mathbf{x}) &= \sqrt{D_{mn}} \left\{ n(n+1) \frac{z_n(kr)}{kr} P_n^{|m|}(\cos \theta) e^{jm\varphi} \mathbf{e}_r + \frac{[kr z_n(kr)]'}{kr} \left[\frac{dP_n^{|m|}(\cos \theta)}{d\theta} \mathbf{e}_\theta + jm \frac{P_n^{|m|}(\cos \theta)}{\sin \theta} \mathbf{e}_\varphi \right] \right\} e^{jm\varphi}, \end{aligned} \quad (4)$$

$(\mathbf{e}_r, \mathbf{e}_\theta, \mathbf{e}_\varphi)$ are the unit vectors in spherical coordinates, z_n designates the spherical Bessel functions j_n or the spherical Hankel functions of the first kind h_n^1 , $P_n^{|m|}$ denotes the associated Legendre polynomial of order n and m , and D_{mn} is a normalization constant given by

$$D_{mn} = \frac{2n+1}{4n(n+1)} \cdot \frac{(n-|m|)!}{(n+|m|)!}. \quad (5)$$

Together with the set of regular solutions to Maxwell equations $\{\Psi_v^1, \Phi_v^1\}_{v=1,2,\dots}$ the surface current densities are approximated by fields of discrete sources. \mathbf{e} and \mathbf{h} solve the nullfield equations (3) and the system $\{\mathbf{n} \times \Psi_\mu^1, \mathbf{n} \times \Phi_\mu^1\}_{\mu=1}^\infty$ form a Schauder basis in $\mathcal{L}_{\tan}^2(S)$. A system $\{\psi_i\}_{i=1}^\infty$ is called a Schauder basis of a Banach space X if any element $u \in X$ can be uniquely represented as $u = \sum_{i=1}^\infty \alpha_i \psi_i$, where the convergence of the series is in

the norm of X [21]. This leads to a sequence $\{a_\mu, b_\mu\}_{\mu=1}^\infty$ such that

$$\begin{aligned} \mathbf{e}(\mathbf{y}) &= \sum_{\mu=1}^{\infty} a_\mu \mathbf{n} \times \Psi_\mu^1(k_i \mathbf{y}) + b_\mu \mathbf{n} \times \Psi_\mu^1(k_i \mathbf{y}), \quad \mathbf{y} \in S, \\ \mathbf{h}(\mathbf{y}) &= -j \sqrt{\frac{\epsilon_i}{\mu_i}} \sum_{\mu=1}^{\infty} a_\mu \mathbf{n} \times \Psi_\mu^1(k_i \mathbf{y}) + b_\mu \mathbf{n} \times \Psi_\mu^1(k_i \mathbf{y}), \quad \mathbf{y} \in S. \end{aligned} \tag{6}$$

In the case of localized vector spherical functions the notion of Schauder basis is closely connected with the Rayleigh hypothesis, which says that the series representation of the scattered field in terms of radiating localized vector spherical functions, which uniformly converges outside the circumscribing sphere, also converges on S .

The scattered field outside the circumscribing sphere can be obtained using the representation theorem

$$\mathbf{E}_s(\mathbf{x}) = \sum_{v=1}^{\infty} f_v \mathbf{M}_v^3(k_s \mathbf{x}) + g_v \mathbf{N}_v^3(k_s \mathbf{x}), \tag{7}$$

$$\begin{aligned} f_v &= \frac{jk_s^2}{\pi} \int_S \left[\mathbf{e}(\mathbf{y}) \cdot \mathbf{N}_{\bar{v}}^1(k_s \mathbf{y}) + j \sqrt{\frac{\mu_s}{\epsilon_s}} \mathbf{h}(\mathbf{y}) \cdot \mathbf{M}_{\bar{v}}^1(k_s \mathbf{y}) \right] dS(\mathbf{y}), \\ g_v &= \frac{jk_s^2}{\pi} \int_S \left[\mathbf{e}(\mathbf{y}) \cdot \mathbf{M}_{\bar{v}}^1(k_s \mathbf{y}) + j \sqrt{\frac{\mu_s}{\epsilon_s}} \mathbf{h}(\mathbf{y}) \cdot \mathbf{N}_{\bar{v}}^1(k_s \mathbf{y}) \right] dS(\mathbf{y}), \end{aligned} \tag{8}$$

where \bar{v} is a complex index incorporating $-m$ and n , i.e. $\bar{v} = (-m, n)$.

Expressing the incident field inside a finite region containing S as a series of regular vector spherical functions

$$\begin{aligned} \mathbf{E}_0(\mathbf{x}) &= \sum_{v=1}^{\infty} a_v^0 \mathbf{M}_v^1(k_s \mathbf{x}) + b_v^0 \mathbf{N}_v^1(k_s \mathbf{x}), \\ \mathbf{H}_0(\mathbf{x}) &= -j \sqrt{\frac{\epsilon_s}{\mu_s}} \sum_{v=1}^{\infty} a_v^0 \mathbf{N}_v^1(k_s \mathbf{x}) + b_v^0 \mathbf{M}_v^1(k_s \mathbf{x}) \end{aligned} \tag{9}$$

allows to derive the T-matrix as (3)–(9) show that the relation between the scattered and the incident field coefficients is linear and can be expressed by a transition matrix \mathbf{T} ,

$$\begin{bmatrix} f_v \\ g_v \end{bmatrix} = \mathbf{T} \begin{bmatrix} a_v^0 \\ b_v^0 \end{bmatrix} \tag{10}$$

with

$$\mathbf{T} = \mathbf{B} \mathbf{A}^{-1}, \tag{11}$$

\mathbf{A} and \mathbf{B} are block matrices

$$\mathbf{B} = \begin{bmatrix} B_{v\mu}^{11} & B_{v\mu}^{12} \\ B_{v\mu}^{21} & B_{v\mu}^{22} \end{bmatrix}, \quad \mathbf{A} = \begin{bmatrix} A_{v\mu}^{11} & A_{v\mu}^{12} \\ A_{v\mu}^{21} & A_{v\mu}^{22} \end{bmatrix}, \quad v, \mu = 1, 2, \dots \tag{12}$$

Explicit expressions for the block elements of matrices \mathbf{A} and \mathbf{B} are given by

$$\begin{aligned} A_{v\mu}^{11} &= \int_S [(\mathbf{n} \times \mathbf{M}_\mu^1) \cdot \mathbf{M}_v^3 + M(\mathbf{n} \times \mathbf{N}_\mu^1) \cdot \mathbf{N}_v^3] dS, \\ A_{v\mu}^{12} &= \int_S [(\mathbf{n} \times \mathbf{N}_\mu^1) \cdot \mathbf{M}_v^3 + M(\mathbf{n} \times \mathbf{M}_\mu^1) \cdot \mathbf{N}_v^3] dS, \\ A_{v\mu}^{21} &= \int_S [(\mathbf{n} \times \mathbf{M}_\mu^1) \cdot \mathbf{N}_v^3 + M(\mathbf{n} \times \mathbf{N}_\mu^1) \cdot \mathbf{M}_v^3] dS, \\ A_{v\mu}^{22} &= \int_S [(\mathbf{n} \times \mathbf{N}_\mu^1) \cdot \mathbf{N}_v^3 + M(\mathbf{n} \times \mathbf{M}_\mu^1) \cdot \mathbf{M}_v^3] dS, \end{aligned} \tag{13}$$

$$\begin{aligned}
B_{\nu\mu}^{11} &= \frac{jk_s^2}{\pi} \int_S [(\mathbf{n} \times \mathbf{M}_\mu^1) \cdot \mathbf{N}_\nu^3 + M(\mathbf{n} \times \mathbf{N}_\mu^1) \cdot \mathbf{M}_\nu^3] dS, \\
B_{\nu\mu}^{12} &= \frac{jk_s^2}{\pi} \int_S [(\mathbf{n} \times \mathbf{N}_\mu^1) \cdot \mathbf{N}_\nu^3 + M(\mathbf{n} \times \mathbf{M}_\mu^1) \cdot \mathbf{M}_\nu^3] dS, \\
B_{\nu\mu}^{21} &= \frac{jk_s^2}{\pi} \int_S [(\mathbf{n} \times \mathbf{M}_\mu^1) \cdot \mathbf{M}_\nu^3 + M(\mathbf{n} \times \mathbf{N}_\mu^1) \cdot \mathbf{N}_\nu^3] dS, \\
B_{\nu\mu}^{22} &= \frac{jk_s^2}{\pi} \int_S [(\mathbf{n} \times \mathbf{N}_\mu^1) \cdot \mathbf{M}_\nu^3 + M(\mathbf{n} \times \mathbf{M}_\mu^1) \cdot \mathbf{N}_\nu^3] dS
\end{aligned} \tag{14}$$

with refractive index $M = \sqrt{\epsilon_i/\epsilon_s}$.

By the far field computed from the far-field pattern \mathbf{E}_{s0}^N for an unit amplitude incident electric field for p- or s-polarization the normalized differential scattering cross section (DSCS) can be obtained:

$$\frac{\sigma_d}{\pi a^2} = \frac{|k_s \mathbf{E}_{s0}^N|^2}{\pi |k_s a|^2}. \tag{15}$$

Orientation averaged scattering is computed by integrating the value of interest $f(\alpha, \beta, \gamma)$ — α, β, γ are the Euler angles—over all directions and polarizations of the incident plane wave using a step wise procedure where the triple integral is converted to three summations.

$$\int_0^{2\pi} \int_0^\pi \int_0^{2\pi} f(\alpha, \beta, \gamma) d\alpha \sin \beta d\beta d\gamma \approx \sum_{n_\alpha=1}^{N_\alpha} \sum_{n_\beta=1}^{N_\beta} \sum_{n_\gamma=1}^{N_\gamma} f(\alpha, \beta, \gamma) \sin(n_\beta \pi / N_\beta) \frac{n_\alpha 2\pi n_\beta \pi n_\gamma 2\pi}{N_\alpha N_\beta N_\gamma}. \tag{16}$$

Angle α is digitized for N_α steps in the range $(0, 2\pi)$, angle β is digitized for N_β steps in the range $(0, \pi)$ and angle γ is digitized for N_γ steps in the range $(0, 2\pi)$.

3. Creating the rough particle

In this paper the focus is on non-symmetrical, rough particles. Usually Gaussian random noise (GRN) is used to create corresponding input shape data. In our work we chose a different way. A long term goal is the application of the NFM-DS to realistically shaped particles, e.g. sprayed metal particles, pollen or spores. For this it is necessary to reconstruct the shape of such particles into computable models. Usually the result will be a three-dimensional grid model. For this reason we use such grid models as base for our light scattering simulations.

To create corresponding input data we use the HyperFun Polygonizer. HyperFun is a simple geometric modeling language. It is intended to model geometric objects described in a function representation (F-rep):

$$F(x_1, x_2, x_3, \dots, x_n) \geq 0. \tag{17}$$

The language is applicable to modeling algebraic and skeleton-based ‘implicit’ surfaces, convolution surfaces, distance-based models, voxel objects, and more general F-rep objects [17]. It polygonizes and displays an object from a file containing a simple command-line language. There also exists a great number of pre-defined object-classes like sphere, ellipsoid, cylinder, torus, etc. which simplify the use. For our case of modeling a rough particle it especially offers a routine which deforms the surface of a given particle shape by putting some noise on it. This routine is called *hfNoiseG(x, amp, freq, phase)*; here the x marks a point coordinates array, *amp* gives the noise amplitude, *freq* designates the noise frequency and the *phase* values suppresses a tartan-like regularity of the pattern. The algorithm behind this *hfNoiseG* library routine is based on the Gardner Series, which was introduced to create a realistic, irregular illustration of a cloudy sky in computer graphics [30,31]:

$$T(X_s, Y_s, Z_s) = \sum_{i=1}^n \frac{c_i}{2} [\sin(\omega_i X_s + P X_i) + 1] \sum_{i=1}^n \frac{c_i}{2} [\sin(\omega_i Y_s + P Y_i) + 1]. \tag{18}$$

The series is used as a mathematical texturing function. Gardner [30] suggests how to define the different elements in the series to get natural-looking patterns. HyperFun uses a slight modification of the series for practical reasons. Therefore we concentrate on the effects caused by the hfNoiseG library routine (as kind of ‘black box’) on the surface of a sphere. We would like to call the parameters *x*, *amp*, *freq* and the *phase* as ‘noise parameters’ from now on. If all these values are set to 0 the result will be the basic shape without any roughness. For this work we choose a sphere as basic shape because it is the most simple structure and so the influence of a rough surface should be easy to determine. To make the surface irregular we use noise parameters of 1.2, 1.4, 1.6 and 1.8 for the amplitude and values of 1.0, 1.2, 1.4, 1.6 and 1.8 for the frequency. The phase shift we did not change, here we use a value of 1.4 which delivers a quite good irregular pattern. Fig. 2 gives an impression of the different mutations of the sphere and graphically elucidates the influence of the noise parameters.

The first particle with amplitude 1.2 and frequency 1.0 is just a slightly modified sphere. Amplitudes equal or larger than 1.8 lead to some kind of disintegration of the surface. Another observation: obviously the phase shifting part of the series has no influence on the starting condition. A closer look on the shapes in one line—same frequency, but different amplitudes—shows that the bulges and the inlets appear at the same positions, only the size changes. This is a positive fact because it allows to compare scattering simulation results for different amplitudes easily.

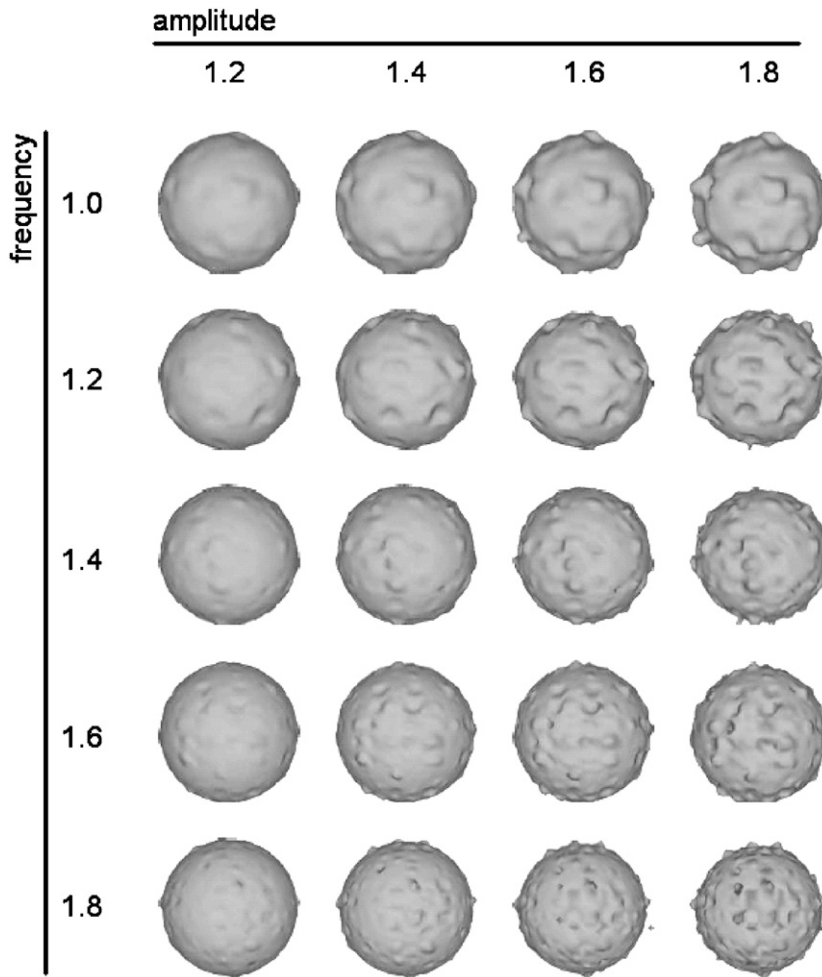


Fig. 2. Overview of the influence of the different values of noise parameters. Different values for the amplitude are arranged horizontally; from left to right: 1.2, 1.4, 1.6, 1.8. Different values for the frequency are arranged vertically; from top to bottom: 1.0, 1.2, 1.4, 1.6, 1.8.

Additionally HyperFun is able to write the computed shape model into a *.wrl* Virtual Reality Modeling Language data file. This format can be converted into the Silicon Graphics WaveFront 3D *.obj* format, which can be read by the light scattering software used for this work.

For this publication we concentrate on selected particles and their corresponding light scattering simulation results from Fig. 2. We leave out particles with too high values for amplitude and frequency as they show disintegration effects on the surface.

4. Numerical results

First we would like to prove the validity of the NFM-DS algorithm and the used program. For this we calculate light scattering by a rough sphere and compare the result to that of a different program using a different scattering theory. In this case we use the commercial *CST Microwave Studio* program [32] for validation, which is based on the finite integration technique (FIT) [33]. For the comparison we choose noise parameters 1.4 for both amplitude and frequency (see Fig. 2) which leads to a particle with some distinct but not too extreme rough surface. Fig. 3 shows that there is a very good correlation between the results of both programs. This means that the NFM-DS algorithm used for our work is capable to calculate light scattering by three-dimensional, non-symmetrical, rough objects.

Now the deformation of the surface has an effect on the particle's volume, which has influence on the scattering diagram. To estimate this we use a *CST Microwave Studio* option that allows to numerically determine the volume of the rough particle. Our investigations show that the volume decreases about $0.05\% \pm 0.02\%$ compared to the original smooth sphere that is deformed. The influence on scattering diagrams caused by this decrease of volume is much lower than the effects caused by the rough surface. Nevertheless this was taken into account for the following results.

Next, one has to consider that the resolution of the particle shape data influences the scattering results, as it was demonstrated by Hellmers [34]. This we would like to check for a particle with noise parameters 1.6 for both the amplitude and frequency. This particle has strong elevations and troughs while still not showing signs of disintegration caused by too high frequency (see Fig. 2). The corresponding light scattering results are shown in Fig. 4.

One can see that the resolution has some influence; on the other side it is only a shift in intensity, the position of minima and maxima due to the scattering angle is constant. A closer look shows that the scattering curves with 5012 and a larger number of surface patches are identical. The most deviating curve comes from the lowest resolution of 1796 patches, the next resolution with 3284 patches is somewhere in between.

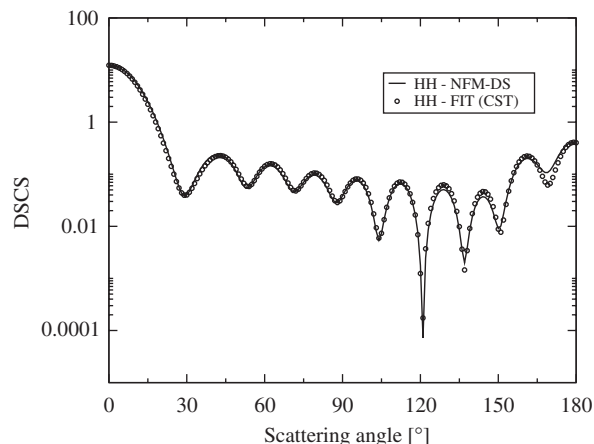


Fig. 3. Differential scattering cross section for a rough sphere, comparison NFM-DS/FIT (CST). $d = 2 \mu\text{m}$, $M = 1.5$, $\lambda = 628.31 \text{ nm}$. Noise parameter: amplitude = 1.4, frequency = 1.4. $N_{\text{rank}} = 20$, $M_{\text{rank}} = 12$ in both cases. N_{rank} is the maximum expansion order that determines the dimension of the T-matrix and M_{rank} is the maximum azimuthal order that determines the number of azimuthal modes. Both have influence on the convergence of the T-matrix results.

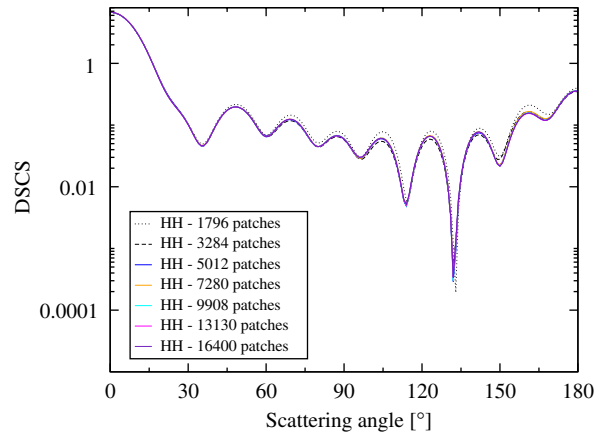


Fig. 4. Differential scattering cross section for a rough sphere, same model created with different degrees of resolution. $d \approx 2 \mu\text{m}$, $M = 1.5$, $\lambda = 628.31 \text{ nm}$. $N_{\text{rank}} = 20$, $M_{\text{rank}} = 12$. Noise parameter for amplitude = 1.6 and frequency = 1.6.

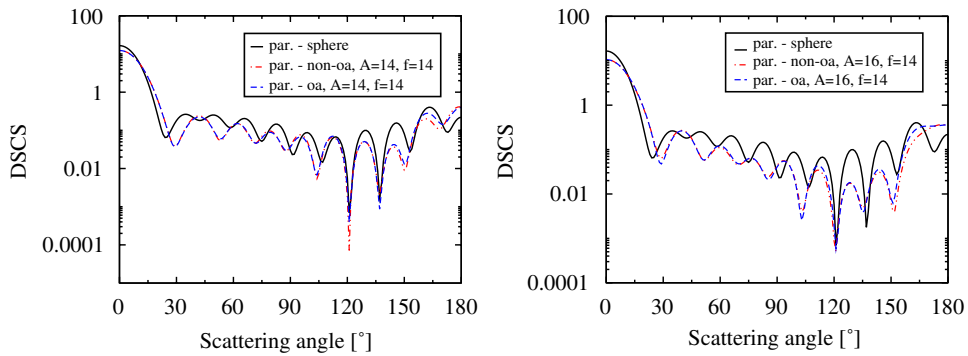


Fig. 5. Comparison of differential scattering cross sections for rough spheres, orientation average versus no orientation average. $d \approx 2 \mu\text{m}$, $M = 1.5$, $\lambda = 628.31 \text{ nm}$. $N_{\text{rank}} = 20$, $M_{\text{rank}} = 12$. Left: noise parameters for amplitude = 1.4 and frequency = 1.4. Right: noise parameters for amplitude = 1.6 and frequency = 1.4.

Altogether the influence seems to be not so critical as one might have expected. Obviously in this case a surface resolution of about 5000 patches would be suitable. The following simulations were done using a resolution between 7000 and 7500 surface patches to be on the same side.

Now one will expect that only for a smooth sphere the direction of incident light has no influence on the scattering pattern. For a rough sphere on the other side it should be wrong to neglect this. Therefore orientation averaging must be done. The orientation of the particle should get more and more influence, the less smooth the simulated particle appears. To consider this we have to calculate the orientation average of the scattered light. To give an impression of this effect and to have a closer look, Fig. 5 shows a comparison of the scattering spectra. It is interesting to see that there is nearly no change in the scattering patterns for the rough sphere. But this changes with different refractive indices. As we are interested in light scattering by small metal droplets, Fig. 6 shows results for the same geometry using a refractive index of $2.7 + 4.27i$ at $\lambda = 578 \text{ nm}$, which corresponds with the optical properties of V2A steel (Fe with 18% Cr and 8% Ni) [35].

Here a clear difference between non-orientation averaged compared to orientation averaged light scattering calculation can be noticed. Especially two observations can be made from Fig. 6: first, while the non-orientation averaged patterns differs strongly from that of a smooth sphere, the orientation averaged curve keeps much closer. Second, the higher the amplitude of the surface noise, the bigger the difference between both for non-orientation and orientation averaged case. Both of these observations are reasonable and were expected.

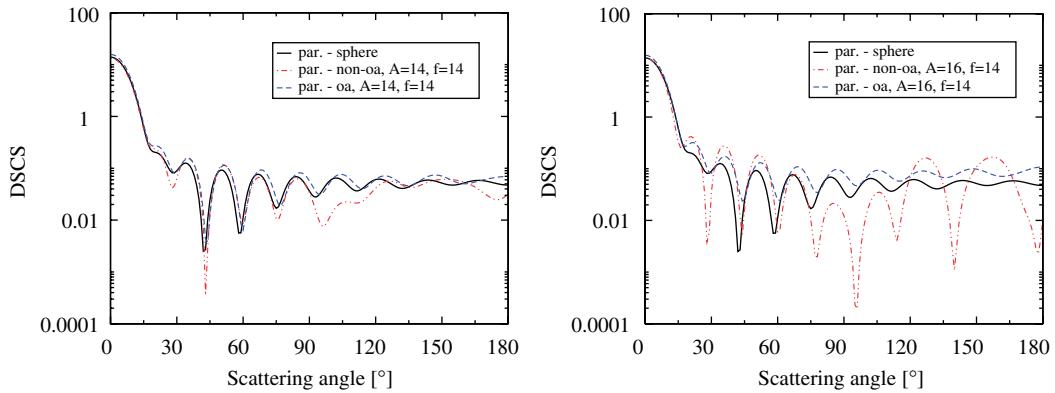


Fig. 6. Comparison of differential scattering cross sections for rough spheres, orientation average versus no orientation average. Material is V2A steel, $d \approx 2 \mu\text{m}$, $M = 2.7 + 4.27i$, $\lambda = 578 \text{ nm}$. $N_{\text{rank}} = 20$, $M_{\text{rank}} = 12$. Left: noise parameters for amplitude = 1.4 and frequency = 1.4. Right: noise parameters for amplitude = 1.6 and frequency = 1.4.

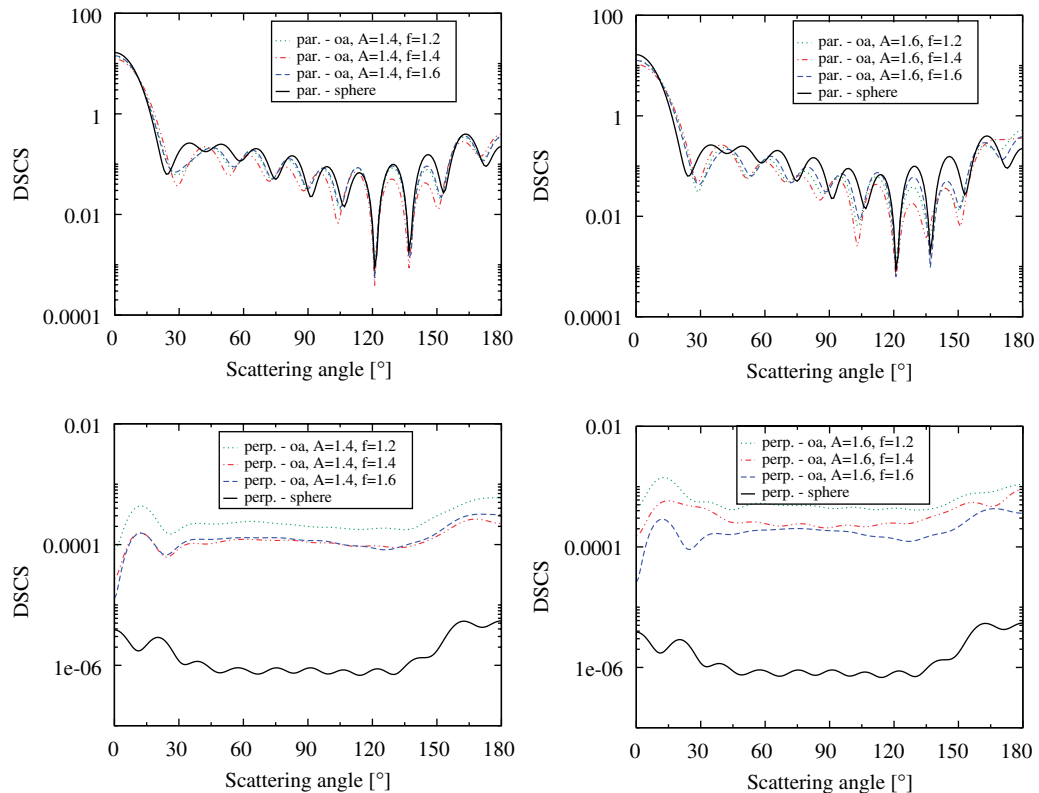


Fig. 7. Differential scattering cross section for a rough sphere (orientation averaged)/same noise amplitude. Top: parallel polarization, bottom: cross polarization. $d \approx 2 \mu\text{m}$, $M = 1.5$, $\lambda = 628.31 \text{ nm}$. $N_{\text{rank}} = 20$, $M_{\text{rank}} = 12$. Left: noise parameter for amplitude = 1.4, right: noise parameter for amplitude = 1.6.

As mentioned above and as one could see from Fig. 2 a characteristic of the Gardner Series is that number and position of bulges and inlets do not change as long as the *phase* parameter does not change. This enables to investigate the influence of different amplitudes with constant frequency and vice versa. For this we calculate the orientation averaged scattering patterns for parallel and cross polarization.

Now a smooth sphere does not show cross polarization. But here we also use a three-dimensional grid model for the shape of the smooth sphere. The discretization of the surface caused by this reconstruction has influence on the scattering diagram [34] and therefore cross polarization can be noticed.

We would like to start comparing scattering diagrams for the same noise amplitudes at different noise frequencies, see Fig. 7.

For the parallel polarization one can see that the number of maxima and minima decreases compared to the smooth sphere. As a result of this, the position of extrema compared to the smooth sphere shifts; among each other the curves for the rough spheres stay close, only varying a bit—with a higher separation at the higher amplitude of roughness. Additionally a characteristic minimum at 120° is obvious. Finally the congruence between all curves is better in backward than in forward direction.

For the cross polarization the difference between smooth and rough surface is much more distinct: the gradient over the scattering angle is absolutely different and the overall intensity is higher for rough surfaces. Comparing the scattering patterns for rough surfaces with each other the trend seems to be, that the lower the frequency the higher the overall intensity. This is reasonable, because a high frequency means more ‘fuzzy’ surface while a low frequency leads to more ‘sharp’ bumps or dints. Apart from that the curves look quite similar.

Now we use the same particle geometries and change the optical properties to those of V2A steel, see Fig. 8. Compared to Fig. 7 one can see that for the parallel polarization DSCS the pattern of the rough spheres correspond much better with that of the smooth sphere, especially in the case of the lower surface roughness 1.4. For the cross polarization it is most notable that the patterns for the rough particles are much more even

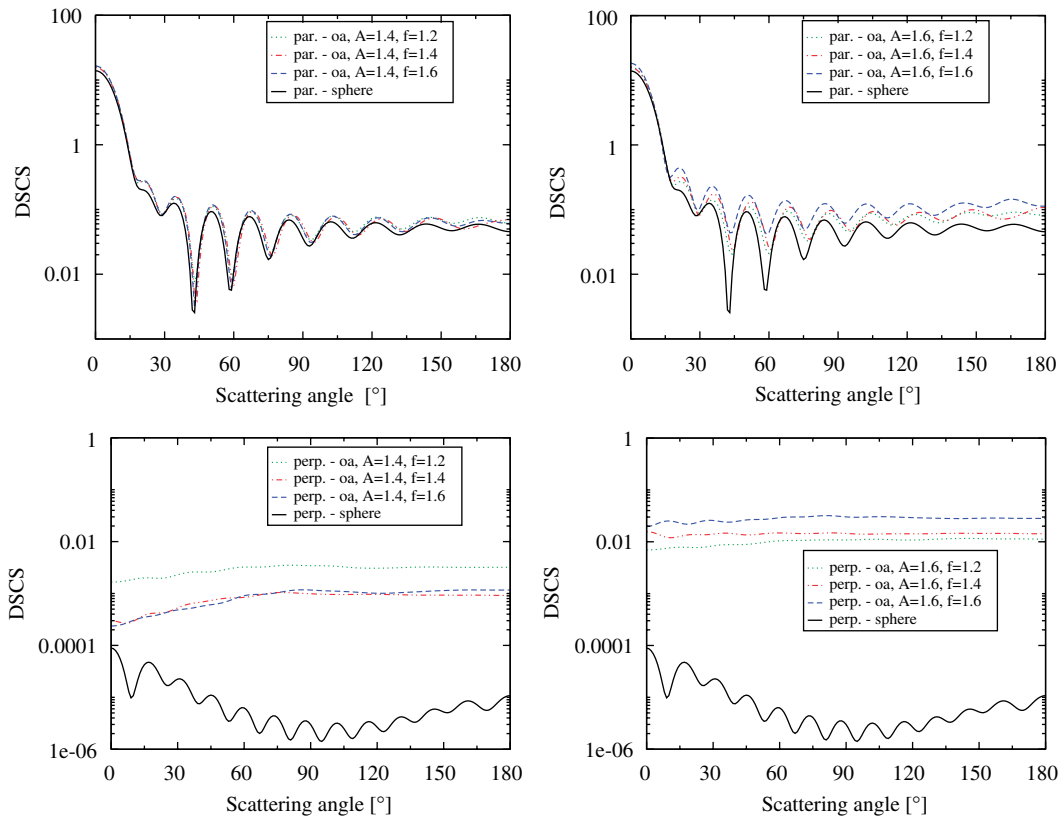


Fig. 8. Differential scattering cross section for a rough sphere (orientation averaged)/same noise amplitude. Top: parallel polarization, bottom: cross polarization. Material is V2A steel, $d \approx 2 \mu\text{m}$, $M = 2.7 + 4.27i$, $\lambda = 578 \text{ nm}$. $N_{\text{rank}} = 20$, $M_{\text{rank}} = 12$. Left: noise parameter for amplitude = 1.4, right: noise parameter for amplitude = 1.6.

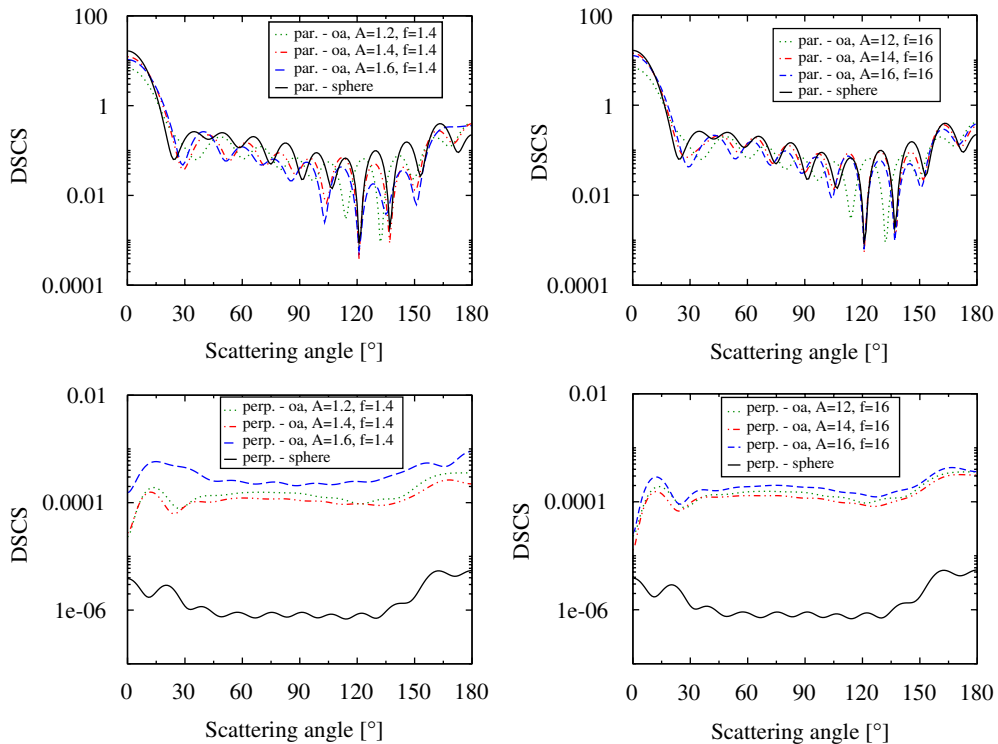


Fig. 9. Differential scattering cross section for a rough sphere (orientation averaged)/same noise frequency. Top: parallel polarization, bottom: cross polarization. $d \approx 2 \mu\text{m}$, $M = 1.5$, $\lambda = 628.31 \text{ nm}$. $N_{\text{rank}} = 20$, $M_{\text{rank}} = 12$. Left: noise parameter for frequency = 1.4, right: noise parameter for frequency = 1.6.

than that in Fig. 7 (amplified by the different range in y -direction). Another observation is that the order of intensities for a surface roughness of 1.6 changes compared to the former case. Here the highest frequency of 1.6 goes along with the highest pattern intensity—while for an amplitude of 1.4 the scattering diagrams corresponds with that of Fig. 7.

Fig. 9 shows the effects of different noise amplitudes at same noise frequencies. Again for the parallel polarization number and position of minima and maxima in light scattering patterns of the rough particles change compared to the smooth sphere. Among each another the positions of the extrema also shift, much stronger than it could be observed in Fig. 7. Also the congruence in backward direction is lost, while the minimum at 120° is obvious again. For cross polarization here it is difficult to come to a conclusion, as in both cases the curve for the lowest amplitude lies between the others. On the other side one can observe that for higher frequencies the scattering patterns start to converge. This again can be attributed to the fact that a higher frequency leads to a ‘fuzzy’ surface.

Fig. 10 now shows the scattering diagrams for the same particle shapes using the optical properties of V2A steel. For the parallel DSCS patterns the observations are the same as in Fig. 8. The differences between rough and smooth shapes are much less than those noticed in Fig. 9, especially for the higher surface roughness of 1.6. Here the patterns for the roughness amplitude parameters 1.2 and 1.4 are nearly identical and very close to that of the smooth sphere. For cross polarization this time there is a different observation: the scattering curves diverge strongly from each other. The curve with the highest surface amplitude of 1.6 in both cases has the highest overall scattering intensity, while for the lowest surface amplitude of 1.2 it is the lowest. These curves even start in the same intensity range as that for the smooth sphere; the following development differs. Both observations are reasonable.

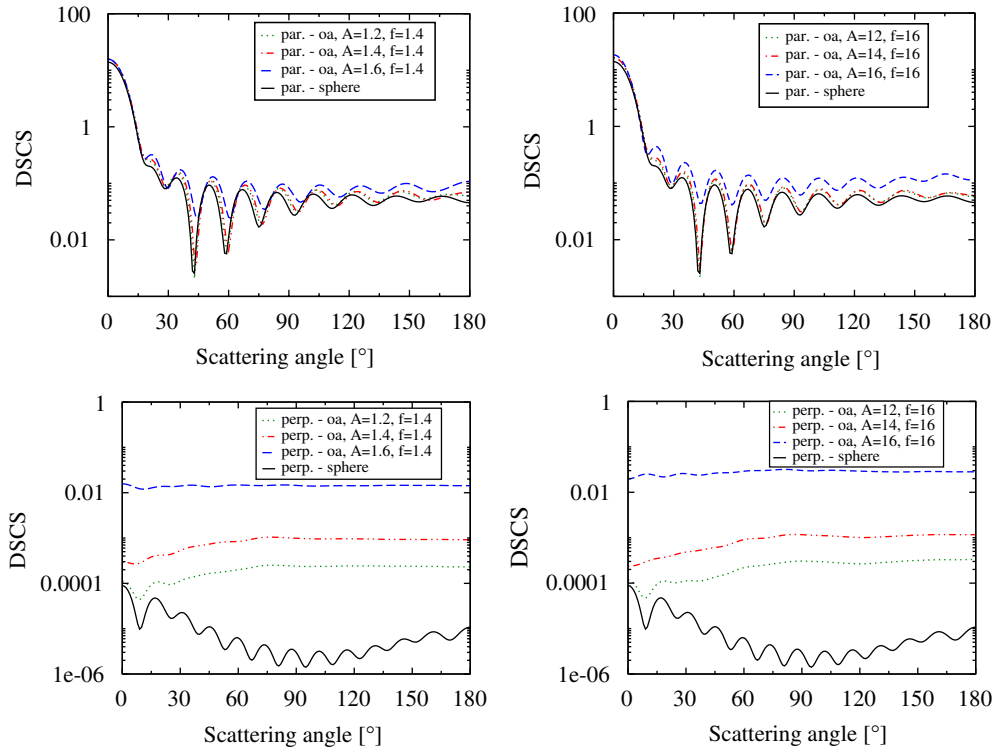


Fig. 10. Differential scattering cross section for a rough sphere (orientation averaged)/same noise frequency. Top: parallel polarization, bottom: cross polarization. Material is V2A steel, $d \approx 2 \mu\text{m}$, $M = 2.7 + 4.27i$, $\lambda = 578 \text{ nm}$. $N_{\text{rank}} = 20$, $M_{\text{rank}} = 12$. Left: noise parameter for frequency = 1.4, right: noise parameter for frequency = 1.6.

5. Summary and conclusions

In this paper we investigate the applicability of the NFM-DS to light scattering simulation for rough spheres and present corresponding scattering results. To create utilizable input shape data for such rough spheres the HyperFun geometric modeling language and its hfNoiseG library routine based on the Gardner Series is used. This software delivers a three-dimensional grid structure as shape input data—which corresponds to data one would get from a three-dimensional reconstruction—that can directly be used as input data for a nullfield approach. By comparing to another algorithm light scattering investigations show that the NFM-DS is capable of calculating light scattering by non-trivial, non-axisymmetrical, rough particle shapes. As the input data is described by a three-dimensional grid structure, the influence of the grid resolution is checked and proved to be less critical than expected. Comparing rough spheres to a smooth one of the same size and optical properties show the influence of the roughness, corresponding light scattering diagrams are presented.

Several conclusions can be made from the results. It is obvious that the cross polarization gives a good clue whether the particle is rough or not. An increasing amplitude of the surface roughness goes along with an increasing overall scattering intensity. This can also be observed in the diagrams for parallel polarization, but in cross polarization it is more distinct. The frequency of the surface roughness on the other side is not so easy to determine from the scattering patterns. Only little effects which partly contradict to each other can be observed.

These conclusions apply to single particle scattering. For scattering by a polydisperse ensemble it is likely that the cross polarization alone provides not enough information about the character of involved particles. Thus this kind of problem requires further investigations, for example by taking into account the orientation average over an ensemble of different particles or the radiative transfer.

In this work, light scattering by single particles with the same shape but different optical properties is investigated. Comparing these results to each other one sees that some of the effects described above become more or less noticeable, depending on the particular scattering problem. This should have influence on later investigations to study light scattering by rough particles, especially if one uses measurements to determine surface characteristics of rough particles. It seems reasonable to estimate results—regarding to optical and surface characteristics—using computational light scattering simulation. For this the NFM-DS as presented in this paper provides to be a useful tool.

Acknowledgment

We would like to acknowledge support of this work by Deutsche Forschungsgemeinschaft DFG.

References

- [1] Eremina E, Wriedt T. Review of light scattering by fiber particles with a high aspect ratio. *Recent Res Dev Opt* 2003;3:297–318.
- [2] Volten H, Munoz E, de Haan JF, Vassen W, Hovenier J, Muinonen K, et al. Scattering matrices of mineral aerosol particles at 441.6 nm and 632.8 nm. *J Geophys Res* 2001;106:13375–417.
- [3] Mann I, Kimura H, Kolokolova L. A comprehensive model to describe light scattering properties of cometary dust. *JQSRT* 2004;89:291–301.
- [4] Doicu A, Wriedt T. Extended boundary condition method with multipole sources located in the complex plane. *Opt Commun* 1997;139:85–91.
- [5] Laitinen H, Lumme K. T-matrix method for general star-shaped particles: first results. *JQSRT* 1998;60:325–34.
- [6] Wriedt T. Using the T-matrix method for light scattering computations by non-axisymmetric particles: superellipsoids and realistically shaped particles. *Part Part Syst Charact* 2002;19:256–68.
- [7] Hovenier JW, Volten H, Munoz O, van der Zande WJ. LBFM waters: laboratory studies of scattering matrices for randomly oriented particles. Potentials, problems, and perspectives. *JQSRT* 2003;79–80C:741–55.
- [8] Kocifaj M, Kapisinsky I, Kundracik F. Optical effects of irregular cosmic dust particle U2015 B10. *JQSRT* 1999;6:1–14.
- [10] Wriedt T, Hellmers J, Eremina E, Schuh R. Light scattering by single erythrocyte: comparison of different methods. *JQSRT* 2006;100:444–56.
- [11] Petrov D, Synelnyk E, Shkuratov YG, et al. Photopolarimetric properties of analytic models of some biological particles with irregular shape. *JQSRT* 2006;102:111–20.
- [12] Maltsev VP, Semyanov KA. Characterisation of bio-particles from light scattering. Utrecht, The Netherlands: VSP; 2004.
- [13] Wriedt T. SEM images of pollen grains. (<http://diogenes.iwt.uni-bremen.de/vt/laser/pollen/pollen.htm>).
- [14] Muinonen K. Light scattering by stochastically shaped particles. In: Mishchenko MI, Hovenier JW, Travis LD, editors. *Light scattering by nonspherical particles*. San Diego: Academic Press; 2000.
- [15] Muinonen K. Light scattering by axially symmetric Gaussian random particles. In: Videen G, Fu Q, Adelphi PC, editors. *Halifax contributions. Fifth international conference on light scattering by nonspherical particles*, MD, August 28–September 1, 2000. p. 91–4.
- [16] Li C, Kattawar GW, Yang P. Effects of surface roughness on light scattering by small particles. *JQSRT* 2004;89:123–31.
- [17] HyperFun (<http://www.hyperfun.org>).
- [18] Waterman PC. Matrix formulation of electromagnetic scattering. *Proc. IEEE* 1965;53:805–12.
- [19] Barber PW, Hill SC. *Light scattering by particles: computational methods*. Singapore: World Scientific; 1990.
- [20] Mishchenko MI, Travis LD. Capabilities and limitations of a current FORTRAN implementation of the T-matrix method for randomly oriented, rotationally symmetric scatterers. *JQSRT* 1998;60:309–24.
- [21] Doicu A, Eremin Y, Wriedt T. *Acoustic and electromagnetic scattering analysis using discrete sources*. San Diego: Academic Press; 2000.
- [22] Doicu A, Wriedt T. Calculation of the T-matrix in the null-field method with discrete sources. *J Opt Soc Am A* 1999;16:2539–44.
- [23] Pulbere S, Wriedt T. Light scattering by cylindrical fibers with high aspect ratio using the null-field method with discrete sources. *Part Part Syst Charact* 2004;21:213–8.
- [24] Hellmers J, Wriedt T, Doicu A. Light scattering simulation by oblate discsphere using the nullfield method with discrete sources located in the complex plane. *J Mod Opt* 2005;53:267–82.
- [25] Hellmers J, Eremina E, Wriedt T. Simulation of light scattering by biconcave Cassini ovals using the nullfield method with discrete sources. *J Opt A* 2005;8:1–9.
- [26] Doicu A, Wriedt T. Null-field method with discrete sources to electromagnetic scattering from layered scatterers. *Comput Phys Commun* 2001;138:136–42.
- [27] Wriedt T, Doicu A. Formulations of the extended boundary condition method for three-dimensional scattering using the method of discrete sources. *J Mod Opt* 1998;45:199–214.
- [28] Wriedt T, Comberg U. Comparison of computational scattering methods. *JQSRT* 1998;60:411–23.
- [29] Müller C. *Foundations of the mathematical theory of electromagnetic waves*. New York: Springer; 1969.

- [30] Gardner GY. Visual simulation of clouds. SIGGRAPH 85. Comput Graphics 1984;19(3):297–303.
- [31] Gardner GY. Simulation of natural scenes using textured quadric surfaces. SIGGRAPH 84. Comput Graphics 1984;18(3):11–20.
- [32] Computer Simulation Technology GmbH (www.cst.de).
- [33] Weiland T. A discretization method for the solution of Maxwell's equation for six-components fields. Electron Commun AEÜ 1977;31:116–20.
- [34] Hellmers J, Wriedt T. Influence of particle shape models on T-Matrix light scattering simulation. JQSRT 2004;89:97–110.
- [35] Hellwege KH, Hellwege AM (eds.). Landolt-Börnstein II. Band: Eigenschaften der Materie in ihren Aggregatzuständen, 8. Teil: optische Konstanten. Berlin: Springer; 1962.